

SCIENTIFIC REPORTS

OPEN

Three-Dimensional Multi-Doped Porous Carbon/Graphene Derived from Sewage Sludge with Template-Assisted Fe-pillared Montmorillonite for Enhanced Oxygen Reduction Reaction

Meiqing Chen^{1,2}, Pingxiao Wu^{1,2,3,4,5}, Liya Chen^{1,2}, Shanshan Yang^{1,2}, Langfeng Yu^{1,2}, Yuefei Ding¹, Nengwu Zhu^{1,4}, Zhenqing Shi^{1,5} & Zehua Liu¹

Three-dimensional multi-doped porous carbon/graphene (Fe-Mt-SS-C) was prepared by carbonization of sewage sludge with template-assisted Fe-pillared montmorillonite. The material consisted of nanosheet- and particle- carbon had a high specific surface area ($784.46 \text{ m}^2 \cdot \text{g}^{-1}$) and hierarchical porous structure of micro-, meso- and macropores. The prepared Fe-Mt-SS-C had a high degree of graphitization and large amount of defect atoms. The pyrolysis process made full use of the C, N, Fe, and S by turning them into the carbon framework of the as-obtained material *in situ*. Template-assisted Fe-pillared montmorillonite contributed to more characteristics of morphology and composition on Fe-Mt-SS-C than other three materials (SS-C, Mt-SS-C and Fe-SS-C), and enhanced the electrocatalytic ORR activity by providing more adsorption sites and the electronic structure, resulting in the increase of conductivity and electrochemical activity. The ORR activity performance of Fe-Mt-SS-C, including the value of onset potential (0.03V) and $E_{1/2}$ (-0.09V), was better than that of commercial 20 wt% Pt/C (-0.02V and -0.18V , respectively). Moreover, the Fe-Mt-SS-C possessed excellent durability and outstanding immunity toward methanol crossover effects. Therefore, the resultant Fe-Mt-SS-C has great potential to applied as a high-efficiency ORR electrocatalyst, more importantly, it realizes the utilization of the sludge at the same time.

With the continuous development of society, energy depletion and environmental pollution get worse. It has no doubt that increasing demands for clean energy¹. The fuel cell with significant advantage stands out². Alkaline fuel cell is a kind of highly potential energy converter with low emission and high efficiency. But cathode catalytic materials of alkaline fuel cell, such as Pt/C catalyst, are expensive and its catalytic activity can't meet the actual demands, which are the main limiting factors in commercialization of alkaline fuel cell³⁻⁵. Therefore, the preparing low cost, excellent activity and high methanol cathode catalytic materials for ORR are the keys to solve the existing problems and achieve the commercialization of fuel cell.

Carbon materials are widely used as cathode catalytic materials in the fuel cell because of their numerous sources, low cost and good stability^{6,7}. A large number of studies have shown that modification by doping with

¹School of Environment and Energy, South China University of Technology, Guangzhou, 510006, P.R. China. ²The Key Lab of Pollution Control and Ecosystem Restoration in Industry Clusters, Ministry of Education, Guangzhou, 510006, P.R. China. ³Guangdong Provincial Engineering and Technology Research Center for Environmental Risk Prevention and Emergency Disposal, South China University of Technology, Guangzhou Higher Education Mega Centre, Guangzhou, 510006, P.R. China. ⁴Guangdong Environmental Protection Key Laboratory of Solid Waste Treatment and Recycling, Guangzhou, 510006, China. ⁵Guangdong Engineering and Technology Research Center for Environmental Nanomaterials, Guangzhou, 510006, China. Correspondence and requests for materials should be addressed to P.W. (email: pppxwu@scut.edu.cn)

metal or nonmetal heteroatoms on carbon materials can achieve optimization of surface performance, so that getting the catalyst with high catalytic activity applies to oxygen reduction reaction⁸. For example, Carbon-based nanomaterials doped metals heteroatoms (Fe, Mn and Co)^{9,10} and nonmetal heteroatoms (N, S, P, etc.)^{11–16} have been observed as promising electrocatalysts for ORR on account of their superior electrocatalytic performance, extraordinary methanol tolerance, remarkable long-term stability, and importantly low cost. Furthermore, many excellent reviews have demonstrated that multi-doped carbon-based nanomaterials (Fe-N-C, S-N-C, P-N-C, etc.)^{17–21} can markedly enhance the ORR activity of carbon-based materials. However, most of the multi-doped carbon nanomaterials were developed by using multiple hazardous chemicals as precursors²². There is thereby an urgent need but it is still a significant challenge to prepare a low-cost multi-doped carbon-based nanomaterial with high ORR performance by utilizing eco-friendly raw material or waste^{23–25}.

With the treatment capacity of sewage greatly increased, urban sludge problem is increasingly outstanding²⁶. Traditional disposal methods of sludge (land sanitary landfill, incineration and Land utilization etc.) not only have the defects of covering a large area, high cost and security risk, but also can't fundamentally realize the "reduction, stabilization, harmless and recycling" of sludge²⁷. Resource utilization is the main trend to solve the problem of sludge. As a result, the conversion of sludge from waste pollutants into the available resources and maximize the value of available components released from the sludge are the ultimate goal of solving the municipal sludge pollution. Sewage sludge consists mainly of organic matter (up to 50–70%), protein and inorganic oxide (containing nitrogen, phosphorus and sulfur)^{28,29}. Sludge pyrolysis can convert it into heteroatoms-doped carbon material, which can be used as a fuel cell cathode catalyst³⁰. There are many excellent studies have investigated the template synthesis strategy in the field of producing micro-/meso-/macroporous carbons with nanoarchitecture^{31–33}. Inorganic solid materials such as zeolites and mesoporous silica have been triumphantly applied as templates to obtain nanoporous carbon materials³⁴. Furthermore, montmorillonite (Mt), especially the modified montmorillonite with expandable interlayer structure and chemical inertness siloxane surface, is thought to be the ideal template in converting carbon-rich organic compounds into three-dimensional carbon nanomaterials^{35,36}. This green technology for recycling of sewage sludge has great research significance and a broad application prospect. However, there is short of relevant research.

In this study, we demonstrated a facile method for developing multi-doped porous carbon/graphene materials for oxygen reduction reaction by using sewage sludge as the sources of carbon and doped heteroatoms, and synergistic effect of template assist from Fe-pillared montmorillonite. The mixture of Fe-pillared montmorillonite and sewage sludge was used to prepare three-dimensional carbon nanomaterial with graphene-style structure. On the one hand, it can make full use of carbon, nitrogen and iron in sludge. On the other hand, it can also take advantage of expandable interlayer structure and the template effect of Fe-pillared montmorillonite. The resultant multi-doped porous carbon/graphene materials had a high specific surface area and doped with heteroatoms exhibited excellent high ORR activity, remarkably ability for immune methanol crossover, and superior durability in alkaline medium, as compared to the other three prepared materials (SS-C, Mt-SS-C and Fe-SS-C) and the commercial 20 wt% Pt/C catalyst. Overall, this study not only puts forward a facile method to prepare multi-doped porous carbon/graphene materials by using sewage sludge as the precursor for oxygen reduction reaction, but also revealed an innovative and green way for sludge recycling use. Preliminary results have shown that the Fe-Mt-SS-C prepared using mixture with $m_{\text{Fe-Mt}}/m_{\text{sludge}}$ of 0.2 and pyrolyzed under 800 °C exhibited more effective oxygen reduction reaction removal than other materials (details are presented in Supporting Material Fig. S1). Fe-Mt-SS-C appeared below was prepared under optimum condition if there was no special instruction.

Results

Morphology and structure analysis. As Fig. 1a illustrated, TOC concentration of supernatant decreases with the increase of the additives (Mt, FeOOH or Fe-Mt)/SS ratios, indicating that Mt, FeOOH and Fe-Mt can adsorb organic compounds in sludge liquid, which has demonstrated in previously research works^{37,38}. The sequence of adsorption capacity was in the following order Fe-Mt > Mt > FeOOH in all additives/SS ratios, suggesting that Fe-Mt can reduce the risk of pollution derived from sludge centrifugal liquid, as well as make full use of carbon source for further pyrolysis.

The analyses of thermogravimetry (TG) on four pyrolysis precursors (SS, Fe-SS, Mt-SS and Fe-Mt-SS) were conducted. As shown in Fig. 1b, there are two mass loss steps: from 30 to 200 °C, the weight loss could be attributed to removal of physically adsorbed water; the gradual mass loss beginning at 200 °C resulted from removal of oxygen-containing functional groups such as OH, C-O, COOH, decomposition of various hydrated compounds and transformation of organic compounds into a carbon material^{11,39,40}. It should be pointed out that the weight loss at each step of Fe-Mt-SS was lower than the other three materials (SS, Fe-SS, Mt-SS), implying that Fe-Mt can maximize preventing the loss of available component in the sludge. The preparation of the Fe-Mt-SS-C followed schematic diagram exhibited as Fig. 1c.

As displayed in Fig. 2a–d, there is obviously difference in the morphologies of the four as-obtained materials (SS-C, Fe-SS-C, Mt-SS-C and Fe-Mt-SS-C). The SS-C mainly forms by a number of carbon particles with diameter of 50 nm and the serious phenomenon of reunion can be found, exhibiting low degree of graphitization. Fe-SS-C and Mt-SS-C primarily consist of nanosheet-carbon with a small amount of particles, indicating that FeOOH and Mt are not only beneficial to the carbonization of the organism in sludge, but also can promote degree of graphitization for carbon. It is worthwhile mentioning that Fe-Mt-SS-C has apparent three-dimensional structure and mainly included uniform graphene-like nanosheets coupled with carbon network composed of tiny particles, which may ascribe to the template assist of Fe-Mt. There were three kind of pore: the macropores generated by removing silicon dioxide in sludge at acid pickling and the stack of graphene-like nanosheets; mesopores and micropores resulted from acid pickling of nano-iron particles on Fe-Mt. A typical TEM image of Fe-Mt-SS-C, as presented in Fig. 2e, indicates overlapping of porous carbon nanosheets in uneven state. Figure 2f reveals the

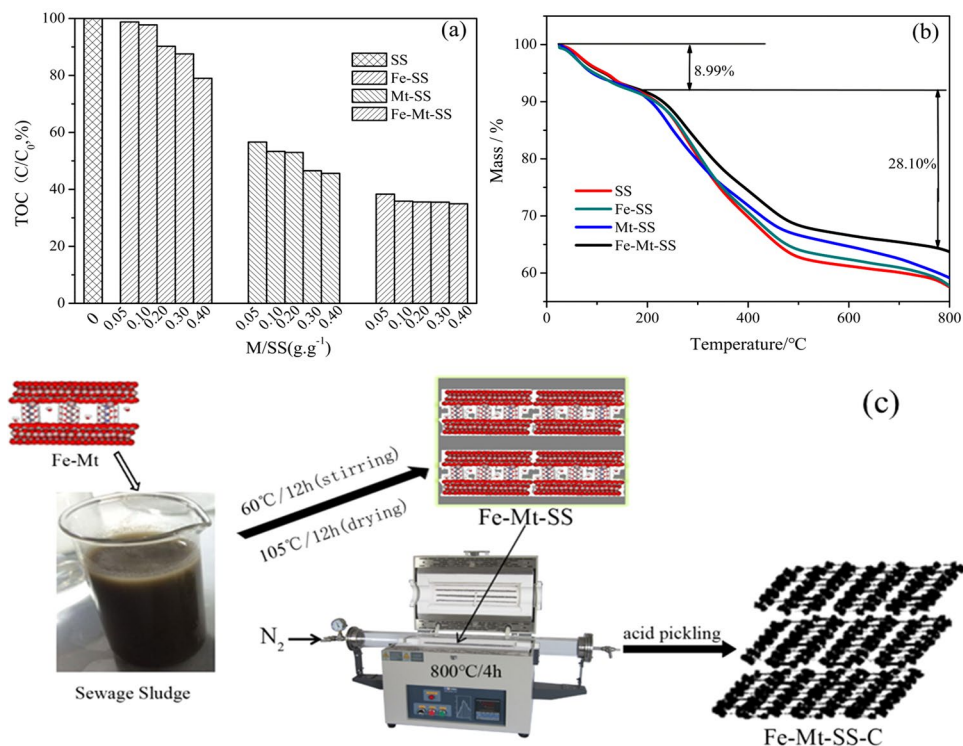


Figure 1. (a) TOC concentration of centrifugation from sewage sludge and after adding difference-proportion Mt, FeOOH and Fe-Mt, (b) TG curves of SS, Fe-SS, Mt-SS and Fe-Mt-SS, (c) schematic diagram of the preparation of the Fe-Mt-SS-C.

lattice spacing of Fe-Mt-SS-C is approximately 0.35 nm that is coincident with the reported results about the lattice spacing of graphene, which further proves the formation of graphene-like nanosheets on Fe-Mt-SS-C^{41,42}.

As illustrated in Fig. 3a, the XRD patterns of four materials (SS-C, Fe-SS-C, Mt-SS-C and Fe-Mt-SS-C) exhibit a peak at 26° labelled as (002) of graphitic-like structure (JCPDS, Card No. 41-2487), while the peak intensity at 26° suggested the degree of graphitization was in the order of Fe-Mt-SS-C > Mt-SS-C > Fe-SS-C > SS-C. Fe-Mt-SS-C appears a peak at approximately 43°, corresponding to the (100) crystal plane, illustrating that the degree in the crystal plane was ordered^{43,44}. Figure 3b shows Raman spectra of the obtained materials, there are two bands at 1355 cm⁻¹ (D-band) related to sp³ defects and 1580 cm⁻¹ (G-band) corresponding to the in-plane vibration of sp² carbon. It was noteworthy that the peak intensity of G-band and the ratio of the D- and G-band intensities (I_D/I_G) on behalf of a quantitative assessment of the defect concentration in carbon materials is with the order of Fe-Mt-SS-C (1.02) > Mt-SS-C (1.01) > Fe-SS-C (1.00) > SS-C (0.97), indicating Fe-Mt-SS-C exists a larger degree of graphitization and a larger amount of defect atoms^{45,46}. The high degree of graphitization and defect structure were ascribed to the contribution of the template effect originated from Fe-Mt. The discoveries of XRD patterns and Raman spectra were consistent with the observation of SEM and TEM.

The adsorption measurements were used to further investigate the feature of the obtained carbon materials. As can be seen from Fig. 4, the N₂ adsorption/desorption analysis isotherm of Fe-Mt-SS-C presented a type IV curve with a gradually increased of positive slope as P/P_0 (0.43–0.98) increased, suggesting that there are good transport properties among the micropores, mesoporous and macroporous channels. The Fe-Mt-SS-C had a BET surface area of 784.46 m²·g⁻¹, according to the Brunauer-Emmett-Teller method, which was higher than that of the other three samples with the order of Fe-Mt-SS-C > Mt-SS-C > Fe-SS-C > SS-C (Table 1). The pore-size distribution curve was illustrated as inset in Fig. 4 and the pore diameters were centered mainly at 1, 3, 5–13, 17 and 30 nm, implying a hierarchical porous structure of Fe-Mt-SS-C that will contribute well to the electrochemical performance because the micropores hold charges, mesopores quicken the kinetic process of ion diffusion, and the open channels of macropores act as ion-buffering depositories^{47–49}. As Table 1 listed, the content of the elements (N, C, S and Fe) on Fe-Mt-SS-C is most compared with the other three obtained materials. Considerable research efforts have found that the introduction of heteroatoms (e.g., N, O, S, Fe, etc.), especially nitrogen, would play a role of promoting in the oxygen reduction reaction^{39,50–52}.

Surface analysis of the prepared materials was detected using X-ray photoelectron spectroscopy (Fig. 5). As Fig. 5a illustrated, the four materials exhibit apparent C1s, O1s, N1s, S2p and Fe2p peaks, in which no Si2p peak is found in the XPS spectrum, indicating SiO₂ had been pickling completely. The corresponding content was listed in the inset table. It must be mentioned that the mass percentages of N1s, S2p and Fe2p in Fe-Mt-SS-C were the least comparing with the other samples (SS-C, Fe-SS-C and Mt-SS-C), which was contrary to the results of Table 1, demonstrating that part of these elements distribute within the carbon frame, which was conducive to oxygen reduction reaction. As Fig. 5b revealed, the most of the carbon in Fe-Mt-SS-C was in the form of

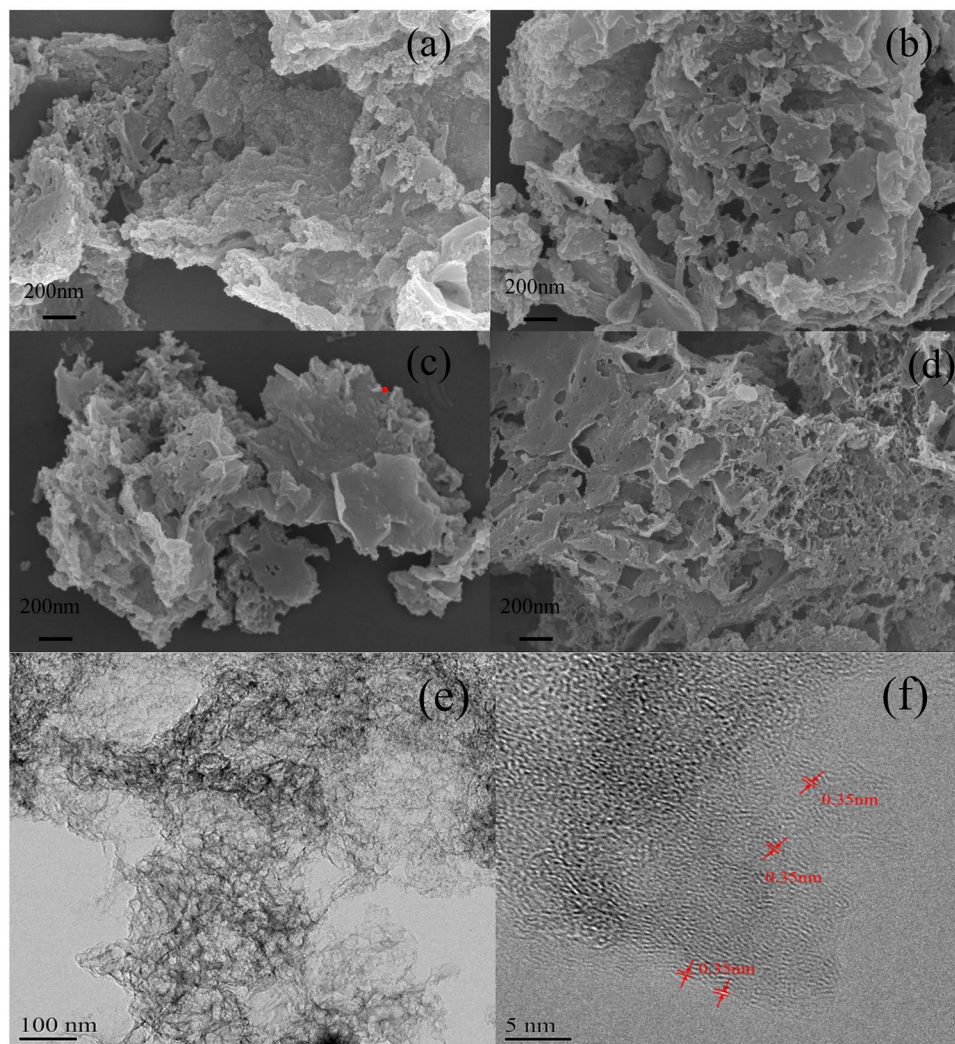


Figure 2. (a–d) FE-SEM images of SS-C, Fe-SS-C, Mt-SS-C and Fe-Mt-SS-C, respectively. (e) TEM image of Fe-Mt-SS-C. (f) HR-TEM image of Fe-Mt-SS-C.

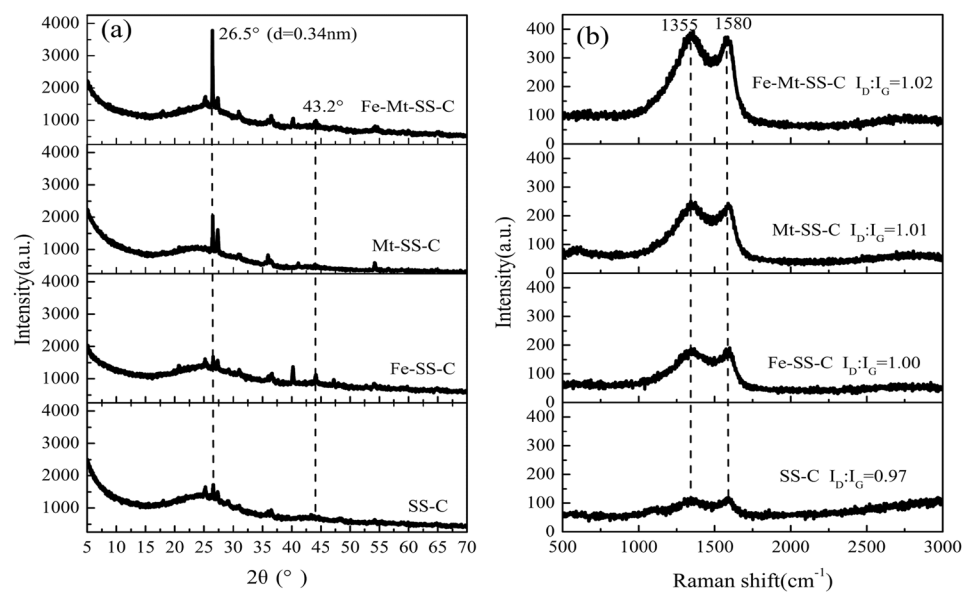


Figure 3. (a) XRD patterns and (b) Raman spectra of SS-C, Fe-SS-C, Mt-SS-C and Fe-Mt-SS-C, respectively.

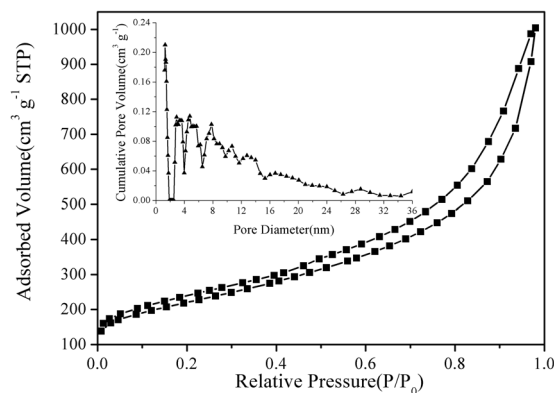


Figure 4. (Inset) pore size distribution and N_2 adsorption-desorption isotherms of Fe-Mt-SS-C.

samples	SS-C	Fe-SS-C	Mt-SS-C	Fe-Mt-SS-C
SBET ($m^2 g^{-1}$)	642.19	650.49	744.07	784.46
average pore size (nm) ^a	5.51	5.80	5.83	7.92
conc. (wt%)				
N ^b	3.25	3.77	3.07	4.48
C ^b	66.40	63.02	61.17	66.48
S ^b	4.70	3.88	3.80	5.67
H ^b	1.49	0.65	0.49	1.20
P ^c	0.57	1.10	1.96	0.14
Fe ^c	1.78	2.29	0.83	4.07
Mg ^c	0.05	0.16	0.05	0.16
Al ^c	1.12	2.04	0.99	2.10
Mn ^c	0.01	0.01	0.01	0.02
Cu ^c	1.72	1.08	0.17	1.11
Ca ^c	0.05	0.07	0.03	0.07
K ^c	0.02	0.02	0.02	0.01
Ni ^c	0.12	0.07	0.02	0.06
Cr ^c	0.14	0.19	0.37	0.23

Table 1. Properties of the as-prepared materials. ^aCalculated from the Barrett-Joyner-Halenda equation using the desorption isotherm. ^bThe contents of C, N, and S were obtained by Elemental Analyze. ^cThe contents of metals were obtained by ICP.

C=C and C-N (Table S1), suggesting that the degree of graphitization was high and this two forms of carbon would play a major role in promoting electrochemical performance⁴⁴. As shown in Fig. 5c, the N1s spectrum exhibits four contributions, pyridinic N, pyrrolic N, graphitic N and pyridinic oxide (pyridinic N⁺-O⁻) located at 398.3 eV, 399.5 eV, 401.5 eV and 402.4 eV, respectively¹². Notably, the content of pyridinic N and graphitic N reached up to 66.5% in Fe-Mt-SS-C (Table S2), the high percentage of pyridinic N and graphitic N was beneficial to oxygen reduction reaction. High-resolution spectra of S in Fe-Mt-SS-C was displayed as Fig. 5d, S2p1/2 and S2p3/2 located at 163.9 eV and 165.2 eV further verified that S atoms were triumphantly doped into the carbon framework⁵³. Moreover, the coexistence of Fe³⁺ and Fe²⁺ is illustrated as Fig. 5e, suggesting Fe hadn't been pickling completely that is favor of boosting the electrochemical performance⁵⁴. Thus it can come to the conclusion that the pyrolysis process made full use of the C, N, Fe, and S by turning them into the carbon framework of Fe-Mt-SS-C, which can provide electrocatalytic active sites, such as C=C, C-N, pyridinic N, graphitic N, C-S-C, etc.

Electrocatalytic properties analysis. The electrocatalytic ORR activity of as-obtained materials was firstly evaluated by cyclic voltammogram (CV) measurements. As depicted in Fig. 6a, Fe-Mt-SS-C illustrates larger double-layer current density than these of SS-C, Fe-SS-C and Mt-SS-C in O₂-saturated 0.1 M KOH, ascribing to the three-dimensional multi-doped porous carbon/graphene with larger surface area as the result of the template-assisted Fe-pillared montmorillonite. Comparative studies of the ORR of as-prepared materials with Pt/C were carried out at the rotation rate of 1600 rpm in O₂-saturated 0.1 M KOH. As exhibited in Fig. 6b, the onset potential is 0.03 V for Fe-Mt-SS-C, -0.02 V for Mt-SS-C and Pt/C, and -0.03 V for Fe-SS-C and SS-C, respectively. And the limiting diffusion current density at -0.4 V increased in the order of 1.76 mA·cm⁻² (SS-C) < 1.81 mA·cm⁻² (Fe-SS-C) < 2.11 mA·cm⁻² (Mt-SS-C) < 2.38 mA·cm⁻² (Fe-Mt-SS-C) < 3.25 mA·cm⁻²

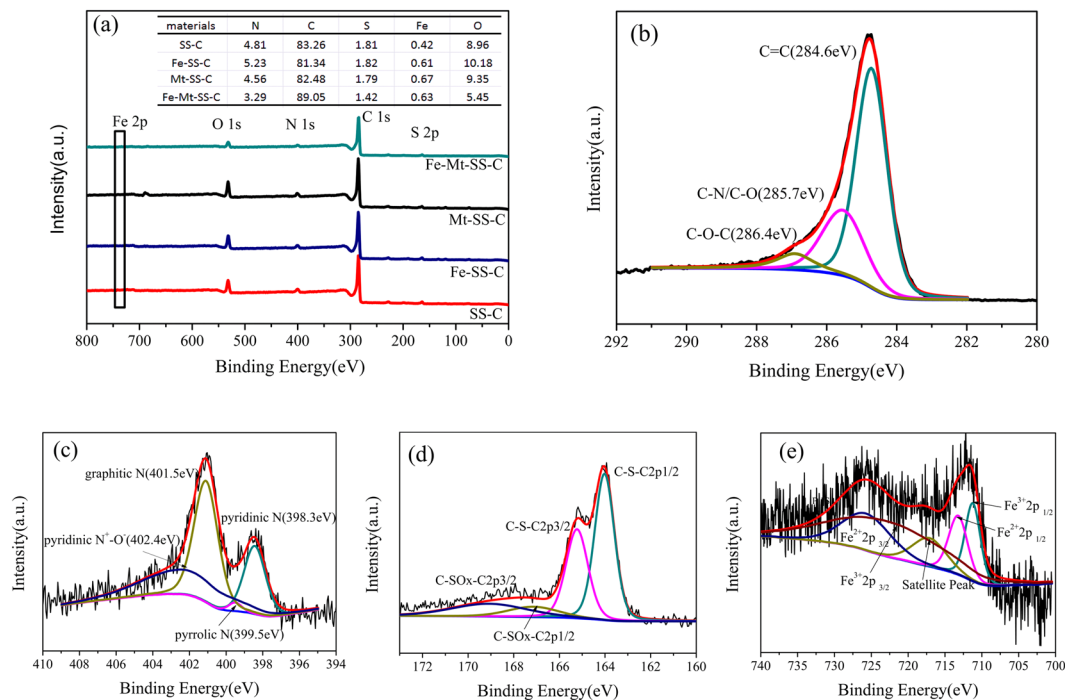


Figure 5. (a) XPS survey of SS-C, Fe-SS-C, Mt-SS-C, Fe-Mt-SS-C and (b–e) high-resolution spectra of C, N, S and Fe in Fe-Mt-SS-C.

(Pt/C). It should be pointed out that the value of the half-wave potential ($E_{1/2}$) of Fe-Mt-SS-C was -0.09 V (vs Ag/AgCl), whereas that of 20 wt% Pt/C was -0.18 V. It can come to a conclusion that the ORR activity performance of Fe-Mt-SS-C, including the value of onset potential and $E_{1/2}$, was better than that of SS-C, Fe-SS-C, Mt-SS-C and commercial 20 wt% Pt/C.

The ORR activity of Fe-Mt-SS-C was estimated by using CV in O_2 - and N_2 -saturated 0.1 M KOH. As shown in Fig. 6c, the Fe-Mt-SS-C displays an oxygen reduction peak at -0.08 V in saturated with O_2 , while in N_2 -saturated 0.1 M KOH, the Fe-Mt-SS-C shows a featureless voltammograms current within the potentials of -1.0 V to 0.2 V (vs Ag/AgCl), which significantly illustrates the ORR activity was effective on Fe-Mt-SS-C electrode in alkaline medium with O_2 ambience. To acquire in-depth knowledge of the electrocatalytic activity on Fe-Mt-SS-C, linear sweep voltammetry (LSV) tests were conducted at given speeds from 100 rpm to 2500 rpm in O_2 -saturated 0.1 M KOH electrolyte. As presented in Fig. 6d, a typical increasing current density with higher rotation speed is displayed, which can be explained by the enhanced oxygen transport at the electrode surface as shortened diffusion distance at high speeds. The result indicated that the ORR of the Fe-Mt-SS-C is diffusion controlled process. The corresponding K-L plots (J^{-1} vs. $\omega^{-1/2}$) obtained from the LSV curves of the Fe-Mt-SS-C exhibited good parallel straight lines (Fig. 6e), indicating a first-order reaction kinetics with the concentration of dissolved oxygen and the same number of transferring electron during ORR at different electrode potentials. On the basis of the slopes gained from the K-L equations, the number of electron transferred was calculated to be about 3.6, reflecting that the ORR was the four-electron route, which was comparable to 20wt% Pt/C catalyst⁵⁵.

The tolerance against methanol crossover of Fe-Mt-SS-C and Pt/C catalysts towards the ORR was investigated by chronoamperometric measurements. As illustrated in Fig. 6f, the methanol crossover of the Fe-Mt-SS-C is significantly different from that of the Pt/C catalyst, which is subjected to a sharp 25% decrease in current when the addition of 3 M methanol into the electrolyte. Notably, the catalytic current density of the Fe-Mt-SS-C exhibits a good tolerance. These findings suggest that the Fe-Mt-SS-C possesses excellent durability and immunity toward methanol effects, thus having potential to apply as a high-efficiency ORR electrocatalyst.

Discussions

The excellent ORR activity of the Fe-Mt-SS-C can be ascribed to the followed three factors. Firstly, the ORR performance of Fe-Mt-SS-C ascribed to high conductivity and electrochemical activity resulted from the 3D structure formed by the nanosheet carbon, the high specific surface area and the porous nature (macropores, mesopores and micropores). Secondly, according to TEM and Raman results, Fe-Mt-SS-C had a high degree of graphitization and large amount of defect atoms assisted the template of Fe-Mt, which served as adsorption sites in ORR^{56,57}. Thirdly, based on the findings of XPS and EA, the C, N, Fe and S had doped into the carbon framework of the as-obtained Fe-Mt-SS-C, which is advantageous to the electronic transmission within the material. The resultant charge separation promotes the adsorption of O_2 over the catalyst and hence improves the ORR property. It had highest total-nitrogen amount and maximal content of pyridinic N and graphitic N that were in favor of oxygen reduction reaction. The coexistence of S and Fe atoms in the carbon framework affected the electronic structure of carbon materials, resulting in the increase of conductivity and electrochemical activity⁵⁸. Thus

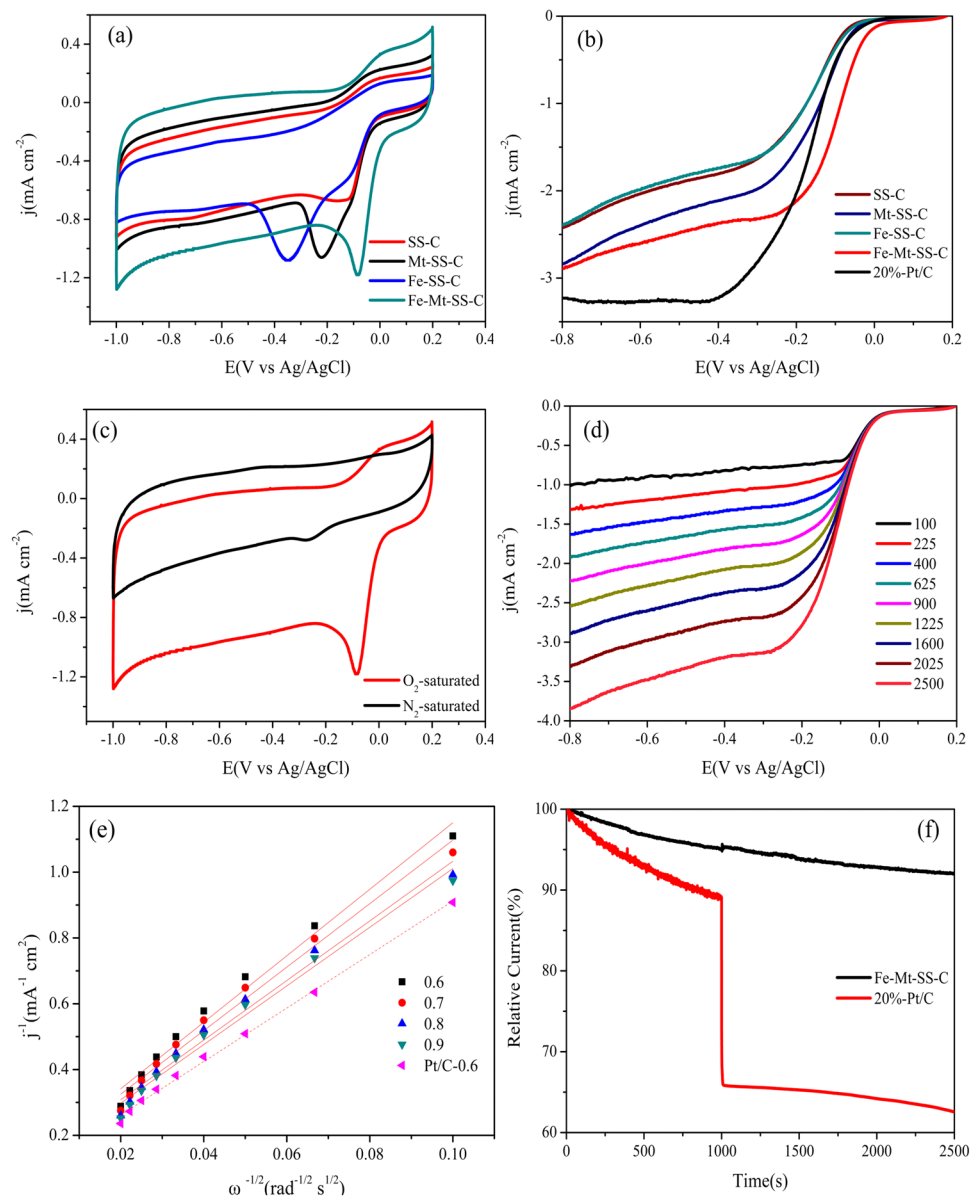


Figure 6. (a) Cyclic voltammograms of as-obtained materials in O_2 -saturated 0.1 M KOH at a scan rate of $10 \text{ mV}\cdot\text{s}^{-1}$; (b) RRDE voltammograms of as-prepared materials and Pt/C at the rotation rate of 1600 rpm. Scan rate: $10 \text{ mV}\cdot\text{s}^{-1}$; (c) Cyclic voltammograms of a Fe-Mt-SS-C in O_2 -saturated and N_2 -saturated 0.1 M KOH at a scan rate of $10 \text{ mV}\cdot\text{s}^{-1}$, respectively; (d) steady state polarization curves of O_2 reduction for Fe-Mt-SS-C in O_2 -saturated 0.1 M KOH at different rotation rates. Ring potential was set at $+0.5 \text{ V}$. Potential scan rate was $10 \text{ mV}\cdot\text{s}^{-1}$. (e) Koutecky-Levich plots of Fe-Mt-SS-C at different electrode potentials. (f) Chronoamperometric responses of Fe-Mt-SS-C and Pt/C electrodes with the addition of 3 M methanol.

it can come to the conclusion that the pyrolysis process take full advantage of the C, N, Fe and S in the sewage sludge by doping them in the carbon framework of the as-obtained material, which can provide electrocatalytic active sites, such as $C=C$, $C-N$, pyridinic N, graphitic N, $C-S-C$, $C-Fe$, etc.^{59,60}. Therefore, the catalytic activity of Fe-Mt-SS-C is much better than that of SS-C, Mt-SS-C and Fe-SS-C. In conclusion, the excellent ORR activity of Fe-Mt-SS-C was due to the synergistic effect of three-dimensional porous structure, a high degree of graphitization with large amount of defect atoms and multi-doped (N, S, and Fe, etc.).

Three-dimensional multi-doped porous carbon containing activated nanoparticles and graphene-like nanosheets were acquired by template-assisted Fe-pillared montmorillonite for sewage sludge via calcination methods. The template-assisted Fe-pillared montmorillonite made a greater contribution to the structure with unique characteristic and the C, N, Fe, and S doping into the carbon framework of Fe-Mt-SS-C than the other three prepared materials (SS-C, Mt-SS-C and Fe-SS-C), and enhance the ORR activity of Fe-Mt-SS-C by providing higher specific surface area and offering more active sites. The value of onset potential (0.03 V) and $E_{1/2}$ (-0.09 V) of Fe-Mt-SS-C was better than that of commercial 20 wt% Pt/C (-0.02 V and -0.18 V , respectively).

The Fe-Mt-SS-C also exhibited outstanding durability and excellent methanol tolerance compared to Pt/C. As a result, the Fe-Mt-SS-C prepared by low-cost method with superior electrochemical performance reveals that the obtained material is good candidate for oxygen reduction reaction, this work may also provide a fundamental and facile method on resource utilization of sludge.

Methods

Materials. Mt used in this study was obtained from Nanhai, Guangdong province, China. Its cation exchange capacity (CEC) and specific surface area is $0.78 \text{ meq}\cdot\text{g}^{-1}$ and $71 \text{ m}^2\cdot\text{g}^{-1}$, respectively. The chemical composition of Mt is 50.8%, 32.4%, 6.75%, 1.86%, 1.7%, 0.09%, 0.72% and 2.07% for O, Si, Al, Mg, Ca, K, Na and Fe, respectively, which was determined by X-ray fluorescence. Sewage sludge sample was supplied by the Lijiao wastewater treatment, located in Guangzhou, China. $\text{Fe}(\text{NO}_3)_3$, Na_2CO_3 , HF (40 wt%) and HCl (37 wt%) were purchased from Guangzhou Chemical Reagent Factory (Guangzhou, P. R. China). All the chemicals were of analytical grade and were used without further purification.

Preparation of Fe-pillared montmorillonite. Fe-pillared montmorillonite was prepared according to our previous report¹⁷. $1 \text{ mol}\cdot\text{L}^{-1}$ Na_2CO_3 solution was added dropwise into $1 \text{ mol}\cdot\text{L}^{-1}$ $\text{Fe}(\text{NO}_3)_3$ solution under magnetic stirring, thermostated at about 65°C for 24 h. The molar ratio of $[\text{OH}^-]/[\text{Fe}^{3+}]$ was 2.0, the hydroxyl solution was slowly added to 2 wt% montmorillonite suspension at a $[\text{Fe}]/\text{clay}$ ratio of $10 \text{ mmol}\cdot\text{kg}^{-1}$, which was prepared in advance in an ultrasonic bath for 30 min, under vigorously stirring. The obtained Fe-pillared montmorillonite suspension was stirred for another 2 h and aged for 24 h at 65°C . The obtained samples were dried at 65°C overnight, ground to 200-mesh, labeled as Fe-Mt.

Preparation of multi-doped porous carbon/graphene materials. 100 ml of sewage sludge suspension with 5%-solid-state rate was mixed with 2 wt% Fe-Mt suspension at a $m_{\text{Fe-Mt}}/m_{\text{sludge}}$ of 0.2. The obtained suspension was stirred at 60°C for 12 h followed centrifugal, and the supernatant was sampled for TOC analysis. The obtained solid mixture was dried at 105°C for 12 h, ground to 200-mesh, noted as Fe-Mt-SS. For comparison, sewage sludge, Mt mixed sludge at a $m_{\text{Mt}}/m_{\text{sludge}}$ of 0.2 (Mt-SS) and iron hydroxyl solution mixed sludge at a $m_{\text{Fe}}/m_{\text{sludge}}$ of 0.2 (Fe-SS) were dealt with the same process. The obtained precursors (SS, Mt-SS, Fe-SS and Fe-Mt-SS) were pyrolyzed in a quartz boat at 800°C for 4 h at a rate of $5^\circ\text{C}\cdot\text{min}^{-1}$ under N_2 flow and cooled down to room temperature. In order to liberate carbon materials, the pyrolysis products were washed by 20 wt% HF followed by 18 wt% HCl for 4 h repeat three times, then filtration and drying. The resulting carbon/graphene materials were donated as SS-C, Mt-SS-C, Fe-SS-C and Fe-Mt-SS-C, respectively.

Characterizations. Thermo-gravimetric and differential scanning calorimetry (TG-DSC) analyses were carried out by using a thermal analysis meter (STA-449F3, Netasch, Germany) under N_2 atmosphere with a heating rate of $5^\circ\text{C}\cdot\text{min}^{-1}$ from 30 to 1000°C . A field emission scanning electron microscopy (SEM, Carl Zeiss, Germany) with an accelerating voltage of 20 kV combined and a transmission electron microscopy (TEM, JEM-3010, JEOL Ltd., Japan) with an accelerating voltage of 200 kV were used to investigate the surface morphology of the materials. The crystalline structure of the products were taken on a D8-Advance X-ray diffractometer, operated on Cu K α radiation ($\lambda = 1.5406 \text{ \AA}$) at 40 kV and 40 mA, with a scan step of 0.02° , a rate of 19.2 s per step and a scan range from 5° to 70° . A FTIR spectrometer (American 96 Thermo-electron Corporation) was used to analyze Fourier-transform infrared (FTIR) spectroscopy, over the spectral range of $4000\text{--}400 \text{ cm}^{-1}$. Raman spectra were obtained on a Renishaw Micro-Raman spectroscopy (Renishaw in Via Reflex) using 514 nm laser excitation. Nitrogen adsorption-desorption experiments for surface and porosity quantification were performed with Chemisorption Surface Area Analyzer (ASAP 2010, Micromeritics, USA). The surface areas were estimated by using the Brunauer-Emmett-Teller method. The X-ray photoelectron-spectras (XPS) analysis were identified by an X-ray photoelectron spectrometer (AES430S, ANELVA, Japan).

Electrochemical measurements. Cyclic voltammetry (CV) and linear sweep voltammetry (LSV) measurements were handled in a three-electrode system on an electrochemical workstation (CHI 660E, Shanghai Chenhua Instrument Co, China) with a rotating disk electrode (RDE) wire. A platinum foil and Ag/AgCl were used as the counter electrode and reference electrode, respectively. The working electrode was prepared as following: The materials (2 mg) were firstly ultrasonically dispersed in ethanol (1 mL) to obtained homodispersed dispersion and then Nafion emulsion ($10 \mu\text{L}$) was added into the dispersion. Secondly, $10 \mu\text{L}$ of the catalyst ink was dropped onto the surface of GC and dried at room temperature for electrochemical test. 20 wt% commercial Pt/C was loaded on the electrode under the same procedure.

References

- Jung, K. *et al.* Rechargeable lithium-air batteries: a perspective on the development of oxygen electrodes. *J. Mater. Chem. A* **4**, 14050–14068 (2016).
- Ghanbarlou, H., Rowshanzamir, S., Parnian, M. J. & Mehri, F. Comparison of nitrogen-doped graphene and carbon nanotubes as supporting material for iron and cobalt nanoparticle electrocatalysts toward oxygen reduction reaction in alkaline media for fuel cell applications. *Int. J. Hydrogen. Energ.* **41**, 14665–14675 (2016).
- Bag, S., Mondal, B., Das, A. K. & Raj, C. R. Nitrogen and Sulfur Dual-Doped Reduced Graphene Oxide: Synergistic Effect of Dopants Towards Oxygen Reduction Reaction. *Electrochim. Acta*. **163**, 16–23 (2015).
- Parvez, K. *et al.* Nitrogen-Doped Graphene and Its Iron-Based Composite As Efficient Electrocatalysts for Oxygen Reduction Reaction. *ACS. Nano*. **6**, 9541–9550 (2012).
- Zhong, X. *et al.* Pt@Au Nanorods Uniformly Decorated on Pyridyne Cycloaddition Graphene as a Highly Effective Electrocatalyst for Oxygen Reduction. *ACS. Appl. Mater. Inter.* **6**, 13448–13454 (2014).
- Zhu, Y. *et al.* A seamless three-dimensional carbon nanotube graphene hybrid material. *Nat. Commun.* **3** (2012).

7. Fang, B., Kim, J. H., Kim, M. & Yu, J. Hierarchical Nanostructured Carbons with Meso-Macroporosity: Design, Characterization, and Applications. *Accounts Chem. Res.* **46**, 1397–1406 (2013).
8. Liu, X. *et al.* High-Performance Electrocatalysts for Oxygen Reduction Based on Nitrogen-Doped Porous Carbon from Hydrothermal Treatment of Glucose and Dicyandiamide. *Chemelectrochem.* **2**, 803–810 (2015).
9. Liao, T., Sun, Z., Kim, J. H. & Dou, S. X. Theoretically Designed Metal-Welded Carbon Nanotubes: Extraordinary Electronic Properties and Promoted Catalytic. *Nano. Energy.* **32**, 209–215 (2017).
10. Oh, H. & Kim, H. The role of transition metals in non-precious nitrogen-modified carbon-based electrocatalysts for oxygen reduction reaction. *J. Power Sources.* **212**, 220–225 (2012).
11. Yang, S. *et al.* A facile method to fabricate N-doped graphene-like carbon as efficient electrocatalyst using spent montmorillonite. *Appl. Clay Sci.* **132–133**, 731–738 (2016).
12. Zhao, J. *et al.* Nitrogen-doped carbon with a high degree of graphitization derived from biomass as high-performance electrocatalyst for oxygen reduction reaction. *Appl. Surf. Sci.* **396**, 986–993 (2017).
13. Zhu, R. *et al.* Templated synthesis of nitrogen-doped graphene-like carbon materials using spent montmorillonite. *Rsc. Adv.* **5**, 7522–7528 (2015).
14. Paraknowitsch, J. P. & Thomas, A. Doping carbons beyond nitrogen: an overview of advanced heteroatom doped carbons with boron, sulphur and phosphorus for energy applications. *Energ. Environ. Sci.* **6**, 2839–2855 (2013).
15. Silva, R., Voiry, D., Chhowalla, M. & Asefa, T. Efficient Metal-Free Electrocatalysts for Oxygen Reduction: Polyaniline-Derived N- and O-Doped Mesoporous Carbons. *J. Am. Chem. Soc.* **135**, 7823–7826 (2013).
16. Sakaushi, K. & Antonietti, M. Carbon- and Nitrogen-Based Porous Solids: A Recently Emerging Class of Materials. *B. Chem. Soc. Jpn.* **88**, 386–398 (2015).
17. Orsmieri, L., Escudero-Cid, R., Videla, A. H. A. M., Ocon, P. & Specchia, S. Performance of a Fe-N-C catalyst for the oxygen reduction reaction in direct methanol fuel cell: Cathode formulation optimization and short-term durability. *Appl. Catal. B. Environ.* **201**, 253–265 (2017).
18. Wu, X. *et al.* Edge-rich and (N, S)-doped 3D porous graphene as an efficient metal-free electrocatalyst for the oxygen reduction reaction. *Rsc. Adv.* **6**, 90384–90387 (2016).
19. Jiang, H. *et al.* Iron Carbide Nanoparticles Encapsulated in Mesoporous Fe-N-Doped Graphene-Like Carbon Hybrids as Efficient Bifunctional Oxygen Electrocatalysts. *ACS Appl. Mater. Inter.* **7**, 21511–21520 (2015).
20. Zhuang, G. *et al.* Synergistic effect of S, N-co-doped mesoporous carbon materials with high performance for oxygen-reduction reaction and Li-ion batteries. *J. Mater. Chem. A.* **3**, 20244–20253 (2015).
21. Choi, C. H., Park, S. H. & Woo, S. I. Phosphorus-nitrogen dual doped carbon as an effective catalyst for oxygen reduction reaction in acidic media: effects of the amount of P-doping on the physical and electrochemical properties of carbon. *J. Mater. Chem.* **22**, 12107–12115 (2012).
22. Jaouen, F. *et al.* Recent advances in non-precious metal catalysis for oxygen-reduction reaction in polymer electrolyte fuel cells. *Energ. Environ. Sci.* **4**, 114–130 (2011).
23. Ranjbar Sahraie, N., Paraknowitsch, J. P., Gobel, C., Thomas, A. & Strasser, P. Noble-metal-free electrocatalysts with enhanced ORR performance by task-specific functionalization of carbon using ionic liquid precursor systems. *J. Am. Chem. Soc.* **136**, 14486–14497 (2014).
24. Chen, P. *et al.* Nitrogen-doped nanoporous carbon nanosheets derived from plant biomass: an efficient catalyst for oxygen reduction reaction. *Energ. Environ. Sci.* **7**, 4095–4103 (2014).
25. Dutta, S., Wu, K. C. W. & Saha, B. Emerging strategies for breaking the 3D amorphous network of lignin. *Catal. Sci. Technol.* **4**, 3785–3799 (2014).
26. Suh, Y. J. & Rousseaux, P. An LCA of alternative wastewater sludge treatment scenarios. *Resour. Conserv. Recy.* **35**, 191–200 (2002).
27. Jin, L., Zhang, G. & Tian, H. Current state of sewage treatment in China. *Water Res.* **66**, 85–98 (2014).
28. Youssef, E. A., Nakhla, G. & Charpentier, P. A. Oleic acid gasification over supported metal catalysts in supercritical water: Hydrogen production and product distribution. *Int. J. Hydrogen. Energ.* **36**, 4830–4842 (2011).
29. Qian, L. *et al.* Treatment of municipal sewage sludge in supercritical water: A review. *Water Res.* **89**, 118–131 (2016).
30. Yuan, S. & Dai, X. Facile synthesis of sewage sludge-derived *in-situ* multi-doped nanoporous carbon material for electrocatalytic oxygen reduction. *Sci. Rep.* **6**, 27570 (2016).
31. Salunkhe, R. R., Kaneti, Y. V., Kim, J., Kim, J. H. & Yamauchi, Y. Nanoarchitectures for Metal–Organic Framework-Derived Nanoporous Carbons toward Supercapacitor Applications. *Accounts Chem. Res.* **49**, 2796–2806 (2016).
32. Dutta, S., Bhaumik, A. & Wu, K. C. W. Hierarchically porous carbon derived from polymers and biomass: effect of interconnected pores on energy applications. *Energ. Environ. Sci.* **7**, 3574–3592 (2014).
33. Malgras, V. *et al.* Nanoarchitectures for Mesoporous Metals. *Adv. Mater.* **28**, 993–1010 (2016).
34. Malgras, V. *et al.* Templated Synthesis for Nanoarchitected Porous Materials. *B. Chem. Soc. Jpn.* **88**, 1171–1200 (2015).
35. Liu, C., Wu, P., Zhu, Y. & Tran, L. Simultaneous adsorption of Cd²⁺ and BPA on amphoteric surfactant activated montmorillonite. *Chemosphere.* **144**, 1026–1032 (2016).
36. Tran, L., Wu, P., Zhu, Y., Liu, S. & Zhu, N. Comparative study of Hg(II) adsorption by thiol- and hydroxyl-containing bifunctional montmorillonite and vermiculite. *Appl. Surf. Sci.* **356**, 91–101 (2015).
37. Feddal, I., Ramdani, A. & Taleb, S. Adsorption capacity of methylene blue, an organic pollutant, by montmorillonite clay. *Desalin. Water Treat.* **52**, 2654–2661 (2014).
38. Galeano, L. A., Ángel, M. & Antonio, V. Treatment of municipal leachate of landfill by Fenton-like heterogeneous catalytic wet peroxide oxidation using an Al/Fe-pillared montmorillonite as active catalyst. *Chem. Eng. J.* **178**, 146–153 (2011).
39. Wang, Q., Jiao, L., Du, H., Wang, Y. & Yuan, H. Fe₃O₄ nanoparticles grown on graphene as advanced electrode materials for supercapacitors. *J. Power Sources.* **245**, 101–106 (2014).
40. Ionita, M., Pandle, M. A. & Iovu, H. Sodium alginate/graphene oxide composite films with enhanced thermal and mechanical properties. *Carbohydr. Polym.* **94**, 339–344 (2013).
41. Liu, X. *et al.* High-Performance Electrocatalysts for Oxygen Reduction Based on Nitrogen-Doped Porous Carbon from Hydrothermal Treatment of Glucose and Dicyandiamide. *ChemElectroChem.* **2**, 803–810 (2015).
42. Chen, Q. *et al.* From used montmorillonite to carbon monolayer–montmorillonite nanocomposites. *Appl. Clay Sci.* **100**, 112–117 (2014).
43. Wang, G. *et al.* Facile Synthesis and Characterization of Graphene Nanosheets. *J. Phys. Chem. C.* **112**, 8192–8195 (2008).
44. Chen, C., Xu, G., Wei, X. & Yang, L. A macroscopic three-dimensional tetrapod-separated graphene-like oxygenated N-doped carbon nanosheet architecture for use in supercapacitors. *J. Mater. Chem. A* **4**, 9900–9909 (2016).
45. Ruiz-Hitzky, E. *et al.* Supported Graphene from Natural Resources: Easy Preparation and Applications. *Adv. Mater.* **23**, 5250–5255 (2011).
46. Zhuang, G. *et al.* Synergistic effect of S, N-co-doped mesoporous carbon materials with high performance for oxygen-reduction reaction and Li-ion batteries. *J. Mater. Chem. A* **3**, 20244–20253 (2015).
47. Yang, M. & Xia, H. Exploration and progress of high-energy supercapacitors and related electrode materials. *Sci. China. Technol. Sci.* **58**, 1851–1863 (2015).
48. Li, Y. *et al.* Polymeric Micelle Assembly for the Smart Synthesis of Mesoporous Platinum Nanospheres with Tunable Pore Sizes. *Angewandte. Chemie. International. Edition.* **54**, 11073–11077 (2015).

49. Li, C. *et al.* Surfactant-Directed Synthesis of Mesoporous Pd Films with Perpendicular Mesochannels as Efficient Electrocatalysts. *J. Am. Chem. Soc.* **137**, 11558–11561 (2015).
50. Zhuang, X., Zhang, F., Wu, D. & Feng, X. Graphene Coupled Schiff-base Porous Polymers: Towards Nitrogen-enriched Porous Carbon Nanosheets with Ultrahigh Electrochemical Capacity. *Adv. Mater.* **26**, 3081–3086 (2014).
51. Huang, D., Luo, Y., Li, S., Wang, M. & Shen, Y. Hybrid of Fe@Fe₃O₄ core-shell nanoparticle and iron-nitrogen-doped carbon material as an efficient electrocatalyst for oxygen reduction reaction. *Electrochim. Acta.* **174**, 933–939 (2015).
52. Wu, X. *et al.* Edge-rich and (N, S)-doped 3D porous graphene as an efficient metal-free electrocatalyst for the oxygen reduction reaction. *Rsc. Adv.* **6**, 90384–90387 (2016).
53. Liang, J., Jiao, Y., Jaroniec, M. & Qiao, S. Z. Sulfur and Nitrogen Dual-Doped Mesoporous Graphene Electrocatalyst for Oxygen Reduction with Synergistically Enhanced Performance. *Angew. Chem. Int. Edit.* **51**, 11496–11500 (2012).
54. Osmieri, L., Escudero-Cid, R., Monteverde Videla, A. H. A., Ocón, P. & Specchia, S. Performance of a Fe-N-C catalyst for the oxygen reduction reaction in direct methanol fuel cell: Cathode formulation optimization and short-term durability. *Applied Catalysis B: Environmental.* **201**, 253–265 (2017).
55. Gao, S., Liu, H., Geng, K. & Wei, X. Honeysuckles-derived porous nitrogen, sulfur, dual-doped carbon as high-performance metal-free oxygen electroreduction catalyst. *Nano. Energy.* **12**, 785–793 (2015).
56. Chen, M., Liu, J., Zhou, W., Lin, J. & Shen, Z. Nitrogen-doped Graphene-Supported Transition-metals Carbide Electrocatalysts for Oxygen Reduction Reaction. *Sci. Rep.* **5**, 10389 (2015).
57. Zhang, L., Niu, J., Li, M. & Xia, Z. Catalytic Mechanisms of Sulfur-Doped Graphene as Efficient Oxygen Reduction Reaction Catalysts for Fuel Cells. *J. Phys. Chem. C.* **118**, 3545–3553 (2014).
58. Dou, S., Huang, X., Ma, Z., Wu, J. & Wang, S. A simple approach to the synthesis of BCN graphene with high capacitance. *Nanotechnology.* **26**, 045402 (2015).
59. Guo, Z. *et al.* Sulfur, Trace Nitrogen and Iron Codoped Hierarchically Porous Carbon Foams as Synergistic Catalysts for Oxygen Reduction Reaction. *ACS Appl. Mater. Inter.* **6**, 21454–21460 (2014).
60. Guo, Z. *et al.* High Performance Heteroatoms Quaternary-doped Carbon Catalysts Derived from Shewanella Bacteria for Oxygen Reduction. *Sci. Rep.* **5**, 17064 (2015).

Acknowledgements

The authors are grateful for financial support from the National Natural Science Foundation of China (Grant Nos 41472038, 41673092, 41273122), the Science and Technology Plan of Guangdong Province, China (No. 2014A020216002, 2016B020242004), Guangdong special support program for millions of leading engineering talents and the Science and Technology Program of Guangzhou, China (No. 201604020064, 201604020055).

Author Contributions

Meiqing Chen, Pingxiao Wu and Nengwu Zhu designed the experiments, Meiqing Chen, Liya Chen, Langfeng Yu and Yuefei Ding performed the experiments, Meiqing Chen, Shanshan Yang, Zhenqing Shi and Zehua Liu analyzed the data. All authors reviewed the manuscript.

Additional Information

Supplementary information accompanies this paper at doi:10.1038/s41598-017-03845-z

Competing Interests: The authors declare that they have no competing interests.

Publisher's note: Springer Nature remains neutral with regard to jurisdictional claims in published maps and institutional affiliations.



Open Access This article is licensed under a Creative Commons Attribution 4.0 International License, which permits use, sharing, adaptation, distribution and reproduction in any medium or format, as long as you give appropriate credit to the original author(s) and the source, provide a link to the Creative Commons license, and indicate if changes were made. The images or other third party material in this article are included in the article's Creative Commons license, unless indicated otherwise in a credit line to the material. If material is not included in the article's Creative Commons license and your intended use is not permitted by statutory regulation or exceeds the permitted use, you will need to obtain permission directly from the copyright holder. To view a copy of this license, visit <http://creativecommons.org/licenses/by/4.0/>.

© The Author(s) 2017